

# Single Photon Counting Large Format Imaging Sensors with High Spatial and Temporal Resolution

Oswald H. W. Siegmund, Camden Ertley, John V. Vallerger,  
*Space Sciences Laboratory, U.C. Berkeley*  
Till Cremer, Chris A. Craven, Alexey Lyashenko, Michael J. Minot  
*Incom Inc., Charlton, MA*

## ABSTRACT

High time resolution astronomical and remote sensing applications have been addressed with microchannel plate based imaging, photon time tagging detector sealed tube schemes. These are being realized with the advent of cross strip readout techniques with high performance encoding electronics and atomic layer deposited (ALD) microchannel plate technologies. Sealed tube devices up to 20 cm square have now been successfully implemented with sub nanosecond timing and imaging. The objective is to provide sensors with large areas (25 cm<sup>2</sup> to 400 cm<sup>2</sup>) with spatial resolutions of <20 μm FWHM and timing resolutions of <100 ps for dynamic imaging. New high efficiency photocathodes for the visible regime are discussed, which also allow response down below 150nm for UV sensing. Borosilicate MCPs are providing high performance, and when processed with ALD techniques are providing order of magnitude lifetime improvements and enhanced photocathode stability. New developments include UV/visible photocathodes, ALD MCPs, and high resolution cross strip anodes for 100 mm detectors. Tests with 50 mm format cross strip readouts suitable for Planacon devices show spatial resolutions better than 20 μm FWHM, with good image linearity while using low gain (~10<sup>6</sup>). Current cross strip encoding electronics can accommodate event rates of >5 MHz and event timing accuracy of ~100 ps. High-performance ASIC versions of these electronics are in development with better event rate, power and mass suitable for spaceflight instruments.

**Keywords:** Microchannel plate, photon counting, imaging, timing

## 1. INTRODUCTION

A general schematic of a microchannel plate (MCP) imaging detector scheme is shown in Fig. 1. In this “sealed tube” ultra-high vacuum device, radiation passes through the input window and is converted to photoelectrons by a photocathode. The photocathode is often a “semitransparent” layer deposited on the inside surface of the window. Another option is an opaque photocathode deposited on the microchannel plate surface. The photoelectrons are amplified by a pair, or a triplet of MCPs, and are then collected by a readout anode consisting of orthogonal patterns of conductive strips. We have used these devices as photon counting, imaging, event time tagging detector schemes for a number of astronomical [1]-[3], remote sensing [4], time resolved biological imaging [5], and night time sensing [6] applications. New photocathode configurations and materials are currently under evaluation, including GaN [7], and UV optimized multialkali cathodes, both in semitransparent and opaque modes. Novel MCPs made by ALD on borosilicate microcapillary arrays (Fig. 2) have many performance characteristics typical of conventional microchannel plates [8]. However, ALD MCPs have shown specific enhancements, low intrinsic background [9](<0.03 events cm<sup>-2</sup> s<sup>-1</sup>), low outgassing during preconditioning [10], and virtually no gain degradation over many C cm<sup>-2</sup> of charge extraction in operation [10]. Additionally, ALD MCPs have ~3x reduced sensitivity to MeV gamma rays, which will reduce background rates in a number of applications [9]. In concert with these developments we have made optimized designs for cross delay line (XDL) and cross strip (XS) image readout anodes and electronics to enable high spatial resolution, timing and enhanced event rates while accommodating large area formats (100 x 100 mm<sup>2</sup>, 200 x 200 mm<sup>2</sup>).

## 2. LARGE FORMAT MICROCHANNEL PLATE DETECTORS

The robustness of borosilicate microcapillary arrays functionalized by ALD techniques as MCPs is enabling the implementation of larger, more stable detectors for Astronomy and remote sensing. Detectors have been developed to cover a wide range of optical/UV sensing applications with formats of 25 mm circular, and 50 mm, 100 mm and 200 mm square have been constructed. Very large focal plane areas were previously unattainable, but the new developments in construction of ALD microchannel plates allow implementation of formats of 20 cm or more. This format can be matched by the readout technologies by extension of the anode structures repetitively and coupling to parallel chains of readout electronics.

To accomplish detailed assessment of 20 cm ALD MCPs we have utilized an open face detector with a 20 cm cross delay line anode for event position encoding (Fig. 3). Encoding the difference in signal arrival times at each end of two orthogonal delay lines allows photon positions in each axis to be determined, and the 400 cm<sup>2</sup> area cross delay line readout has an end to end signal propagation of ~130 ns. The detector scheme provides event by event accumulated images and gain map images for the MCPs that can be used to characterize the efficiency, overall uniformity, background rate and spatial resolution of the 20 cm ALD MCPs when used in a pair or triple stack configuration. The 20 cm detector spatial resolution was assessed with the current generation of time to digital electronics using 13 bit electronic position coordinate binning. With this readout, resolution of <100 μm FWHM has been achieved [11]. In addition, event time tagging to the 100 ps level can be accommodated with parallel timing electronics. Readouts for 50 mm and 100 mm have been accomplished with the XS anode scheme (Fig. 4), providing much higher spatial resolution despite using MCP gain one order of magnitude less.

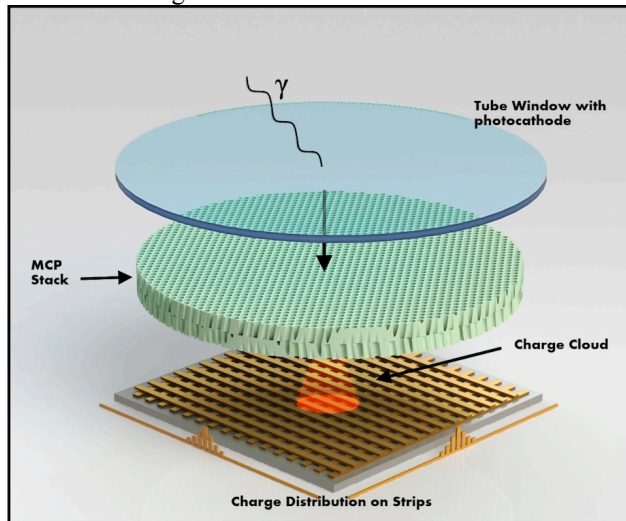


Fig. 1. An MCP imaging sensor scheme. A photocathode is deposited on a window facing a pair of MCPs. Emitted photoelectrons are detected by the MCPs and collected by several strips in each axis of an anode to encode positions.

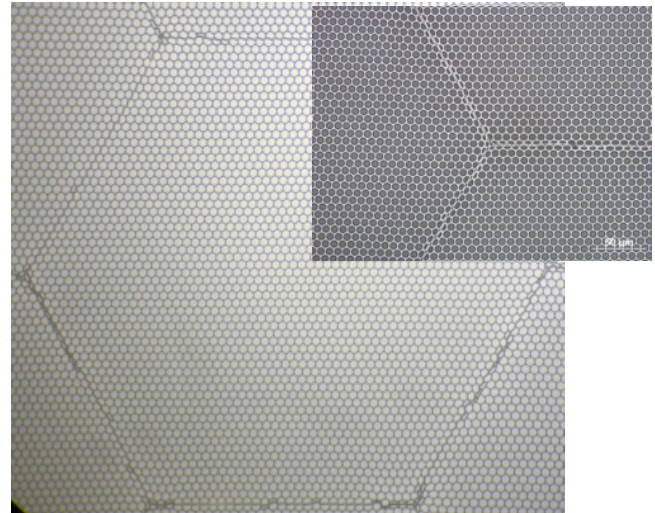


Fig. 2. Uniformity of microchannel plate borosilicate substrates. Left MCP 20 μm pore 74% open area and 13° pore bias angle, right 6 μm pores with a 65% open area, 60:1 pore L/d, and 8° pore bias angle.

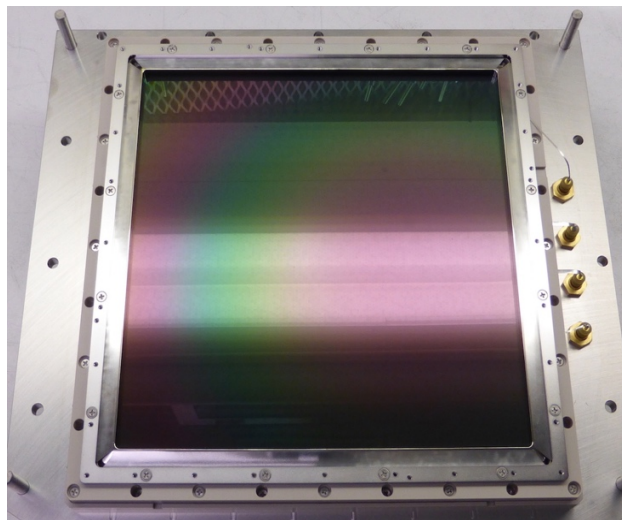


Fig. 3. KBr photocathode deposited onto a 200 × 200 mm ALD borosilicate MCP in a detector with a cross delay line anode readout for sounding rocket UV spectroscopy. (Courtesy- J. Green U. Colorado).

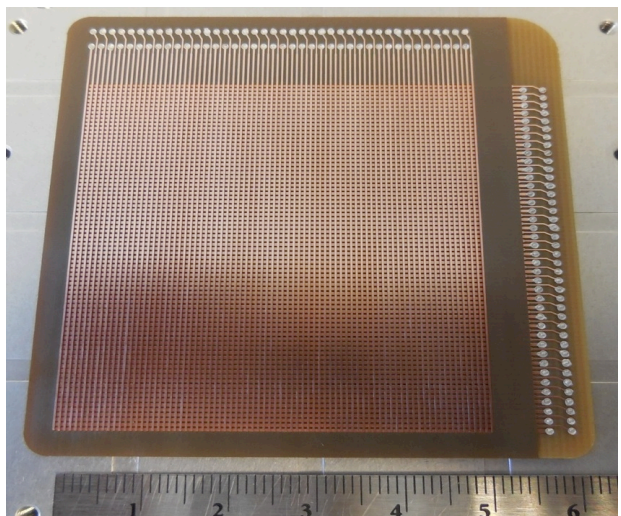


Fig. 4. 50x50 mm XS anode showing the 80x80 strips in each orthogonal axis insulated from each other with polyimide layers. 50% of the charge is captured in each axis and is spread over several strips [12].

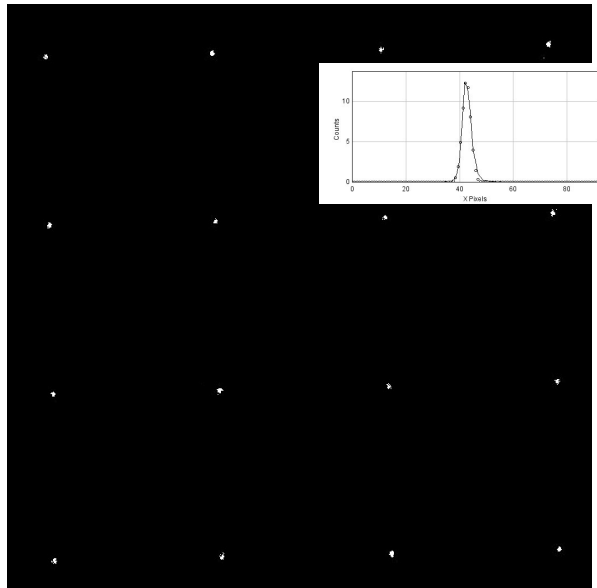


Fig. 5. 50 mm XS anode with PXS-II electronics and a pair of 10  $\mu\text{m}$  pore MCPs operating at  $\sim 1 \times 10^6$  gain. UV image of pinhole mask of 10  $\mu\text{m}$  holes on 1 mm spaces. Inset: PSF of a single hole with 20  $\mu\text{m}$  FWHM. [12]

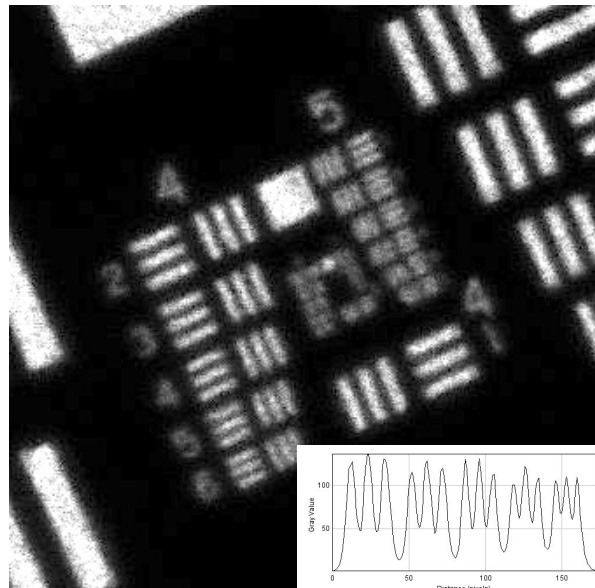


Fig. 6. 50mm XS anode with PXS-II electronics and a pair of 10 $\mu\text{m}$  pore MCPs operating at  $\sim 1 \times 10^6$  gain. UV image of an Air Force Test Pattern mask. Inset is a cut through Group 4. Resolution  $\sim 18\mu\text{m}$  FWHM. [12]

## 2.1 ALD Microchannel Plates

A borosilicate glass micro-capillary array substrate can be configured to function as a microchannel plate by deposition of resistive and secondary emissive layers using atomic layer deposition. This establishes a robust substrate at reduced cost and permits much larger than normal microchannel plates to be produced. Initially glass tubes are stacked and fused together, so no core glass etching is required as in standard MCP fabrication. These MCPs show hexagonal structures (multifibers, Fig. 2) which are the fundamental stacking blocks for the glass tubes. When many multifibers are fused together to make a full size MCP some of the glass tubes (pores) at the hexagonal interfaces deform. Deposition of a uniform resistive layer by ALD allows the application of an accelerating potential across the MCP. A uniform secondary emissive layer is also deposited onto the substrate using ALD, followed by evaporation of NiCr electrodes complete the MCP fabrication process. Both  $\text{Al}_2\text{O}_3$  and  $\text{MgO}$  have been used to achieve the high secondary emission coefficient electron multiplication layers. The robustness and flatness of the MCPs using borosilicate microcapillary arrays is excellent, and is due in part to the resilience and stability of the substrate material and its high temperature properties ( $\sim 700^\circ\text{C}$  softening point for the C14 material currently in use). The resistance of MCPs fabricated so far has a wide range, from  $\text{k}\Omega$  to  $\text{G}\Omega$ . Pore sizes range from 40  $\mu\text{m}$  to 6  $\mu\text{m}$  (Fig. 2) but 20  $\mu\text{m}$  and 10  $\mu\text{m}$  are most common. Bias angles of the pores are  $8^\circ$  or  $13^\circ$ , with pore open area ratios from 65% to 80%,  $\sim 74\%$  being standard. Large MCPs with 200 mm square format have been made in quantity, but many smaller sizes have also been made.

## 2.2 Cross Strip Photon Counting Imaging Readout

The XS anode is made with layers of metals and insulators on an insulating substrate, producing two sets of strips in orthogonal directions. The top and bottom layers have equal exposed areas, and thus collect the charge from the MCPs with equal charge sharing (Fig. 1). The distance between the anode and the MCP stack is typically 2.5 mm, and is optimized for the charge cloud spread of the MCP configuration. Each anode strip is connected to the back side of the anode using hermetically sealed vias allowing mounting of all the detector electronics outside the vacuum. The preamplifier electronics are then connected at the back side of the anode close to the vias (for lower capacitance) to achieve the best noise characteristics and preserve timing properties. Low outgassing materials such as polyimide have been used for XS anodes in open face detectors [12]. These accommodate formats of 25 mm, 50 mm and 100 mm. A representative example of this is the 50mm XS shown in Fig. 4, which shows the two layers of strips and the connection vias.

In the PXS-II [13] XS readout electronics scheme each strip on the anode is connected directly to a preamp input of a set of 32-channel ASICs [12]. The output of these amps are shaped unipolar pulses of  $\sim 50$  ns rise time,  $\sim 500$  ns fall time with a noise floor of  $\sim 500 + 50/\text{pF} \cdot C_{\text{load}}$  electrons. These parallel outputs are amplified again before being continuously digitized by discrete 12-bit analog to digital converters operating at 50 mega-samples per second. The digital

samples are fed into an FPGA (Xilinx Virtex6 family) and are digitally filtered to extract pulse peak information. This identifies also the triggered channels to derive the event centroid for both X and Y axes. This centroid position is combined with the digital timing signal determined by a constant fraction style digital filter. The events are transmitted as an event list of X, Y (up to 14 bits each) and T (with ~20 ps LSB). These have demonstrated resolutions of 18  $\mu\text{m}$  with 50 mm XS anodes (Fig. 5, 6) and 100 mm XS anodes with event rate handling of 5 MHz at <20% deadtime [14]. A new generation of spaceflight capable electronics is currently under development as an ASIC implementation with improved rate limits, and lower power and volume [12].

### 2.3 Performance of ALD coated Microchannel Plates

Tests with 33mm round format ALD MCPs on borosilicate substrates have established [9], [10] that the gain, pulse amplitude distribution, and MCP resistance are similar to conventional MCPs. However, one consequence of high secondary emission ALD coatings is better pulse height saturation leading to narrower pulse amplitude distributions at lower gains [9]. This is helpful in reducing the amplitude range of signals for new high-resolution readouts like the XS which operate at low gain. For large area format MCPs there are often problems with the spatial uniformity of the operating characteristics [10] due to intrinsic variations in the amplification process, and the physical flatness of the MCPs. The C5 and C14 borosilicate substrates that have been fabricated show excellent flatness, and with optimization the ALD layer performance has achieved gain uniformity over 20 cm MCPs that is better than 15% [9].

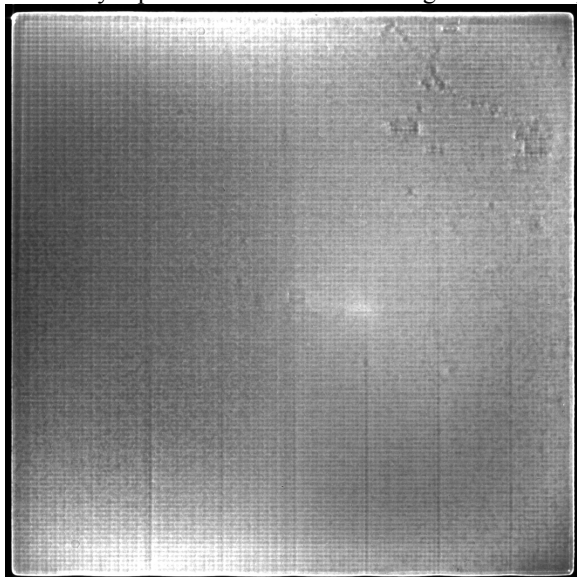


Fig. 7. UV illuminated (184 nm) image for a 10 cm ALD coated MCP pair. Gain  $\sim 1.5 \times 10^6$ , 8  $\mu\text{m}$  pores, 80:1 L/d, using a 100 mm XS with PXS-II imaging electronics.

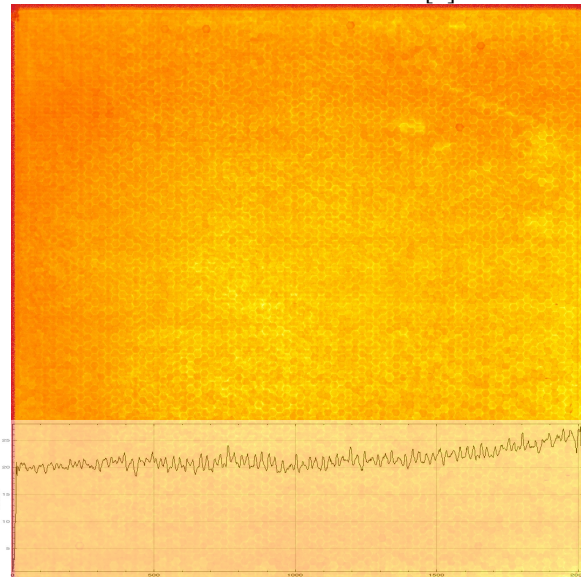


Fig. 8 184 nm illuminated gain map image for a 10 cm 8  $\mu\text{m}$  ALD coated MCP pair, 80:1 L/D, gain  $\sim 1.5 \times 10^6$ , Histogram shows the MCP multifiber gain variations.

We have also used ALD to deposit secondary emissive layers to conventional MCPs with dimensions up to 100 x 100  $\text{mm}^2$ . Tests of these MCPs (Fig. 7, 8) show that the imaging is dominated by readout and MCP substrate features. The image striations in Fig. 7 are residuals of the 100 mm XS anode pattern and the PXS-II readout electronics algorithms. The accompanying gain map image shows the hexagonal MCP packing structure, but the overall gain is flat to ~20%.

ALD borosilicate MCP background rates are exceptional,  $<0.03 \text{ events cm}^{-2} \text{ s}^{-1}$  [9] compared to conventional MCPs [15] due to low intrinsic radioactivity in the glass. Conventional MCP glass formulations have potassium and  $^{40}\text{K}$  beta decay dominates the intrinsic background. There is little  $^{40}\text{K}$  in the C5 or C14 glasses, and the measured background rate is comparable to the expected rate due to cosmic ray muon events. The background spatial distribution has been uniform, even for MCPs of 200 mm size [9]. Another distinguishing property of ALD borosilicate MCPs is their sensitivity to gamma ray background. The absence of lead in the substrate chemistry results in a reduction of MeV gamma ray sensitivities to ~0.7% as opposed to ~2% for standard MCPs [9]. ALD borosilicate MCP UV quantum detection efficiency measurements show a consistently higher efficiency than the best historical [2], [16] conventional MCP efficiencies. Both the increased open area ratio for the ALD substrates, and the high secondary emission coefficients may contribute to this. Subsequent measurements of alkali halide opaque cathodes deposited onto ALD borosilicate MCPs also show parity with the best historical cathode coated conventional MCP efficiencies [16].

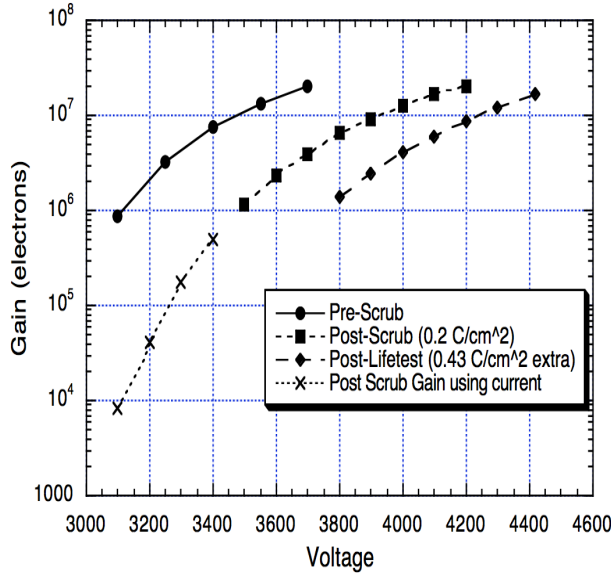


Fig. 9. Burn-in of COS-HST MCPs (12  $\mu\text{m}$  pore, 3 stack, 80:1 L/d, 19° bias) shows almost 2 orders of magnitude gain loss over 0.6  $\text{C cm}^{-2}$  extracted at a burn-in gain of  $\sim 5 \times 10^4$ . [2].

Pre-conditioning steps and gain stability are an important issue for MCP lifetime and detector stability [15]. Conventional MCP pair/triplet gain drops by one to two orders of magnitude during operational burn-in (Fig. 9), and significant adsorbed gas is released. Optimizations of secondary emissive layers ( $\text{Al}_2\text{O}_3$  and MgO) on borosilicate ALD microchannel plates have shown that the cleanliness of the surfaces is very important for ALD MCP gain stability. Generally,  $\text{Al}_2\text{O}_3$  coated MCPs show a decline in gain with charge extraction [10]. If a vacuum bake is performed on MgO coated borosilicate MCPs the gain can remain stable during burn-in up to 7  $\text{C cm}^{-2}$  [10]. The gain remains stable to  $>1 \text{ C cm}^{-2}$  for MgO coated C14 substrate MCPs [9] even after limited air exposure, and gain is recoverable even after long exposures by baking or burn-in of the MCPs. Stability is also not compromised by subsequent exposure to dry  $\text{N}_2$  for 4000 hours [17]. We have also applied MgO ALD layers to conventional MCPs and achieved improved stability. In tests where the MCPs were operated at full gain (1 pC) and very high flux the gain initially drops very rapidly, but only by about 30 to 40% and then remains quite stable (Fig. 10). Subsequently, several days at dry  $\text{N}_2$  does not affect the gain. In both cases, ALD borosilicate and ALD coated standard MCPs, the imaging performance is not noticeably affected.

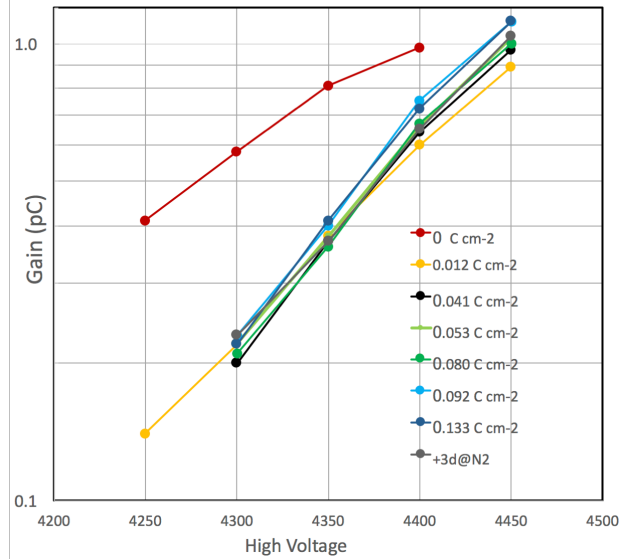


Fig. 10. Burn-in of normal MCPs (46 x 30  $\text{mm}^2$ , 3 stack 12  $\mu\text{m}$  pore, 80:1 L/d, 13° bias) with ALD MgO emissive layer on the bottom MCP. 40% gain loss in less than 0.012  $\text{C cm}^{-2}$  then  $\sim$ stable. (Burn-in gain of  $\sim 7 \times 10^6$ ).

### 3. SEALED TUBES WITH ALD MCPS

The properties of ALD MCPs make them attractive for sealed tube devices with novel photocathode materials. Sealed tubes with ALD MCPs have been made in 200 mm format (Fig. 11), 25 mm round (with an opaque GaN photocathode) [7], [18] and square 50 mm format (Planacon [19]). The 20 cm square format sealed tube detector [20] has been developed by a collaboration (Large Area Picosecond Photon Detector - LAPPD) consisting of Incom. Inc., U. Chicago, Argonne National Laboratory, U. C. Berkeley, U. Hawaii, and several other institutions.

#### 3.1 Large Area 20 cm Sealed Tube Development

The LAPPD program seeks to produce large area flat panel sealed tubes for optical/UV sensing applications in detection of Cherenkov light (RICH), scintillation detection, and neutron imaging. Key requirements are the 20 x 20 cm size, event timing to 10 ps or better and image resolution at the 1 mm scale. The detector is a proximity focused device that is only  $\sim 20$  mm thick (Fig. 11). It comprises a Borofloat 33 input window with a semitransparent bialkali proximity focused photocathode, a pair of 20  $\mu\text{m}$  pore ALD borosilicate MCPs with a biased gap (1 mm), and a  $\sim 5$  mm anode gap to a strip-line anode. Several sealed tubes have been successfully completed. The bialkali photocathodes (KCs:Sb) were deposited onto borosilicate windows in a transfer system and the seals made using hot indium bonding. The best efficiencies exceeded 30% at the shortest wavelengths (Fig. 12) and the uniformity was reasonably good (Fig. 13) given the large 20 cm area of the flat cathode. No changes to the efficiency have been seen over the several months since the completion of this sealed tube. ALD borosilicate MCPs with large area are essential for this project. A comparison of 20 cm MCP pair gain-voltage characteristics for  $\text{Al}_2\text{O}_3$  and MgO secondary emissive layers is shown in Fig. 14 and exemplifies the consistency and effectiveness of MgO as a secondary emitter for ALD MCPs.

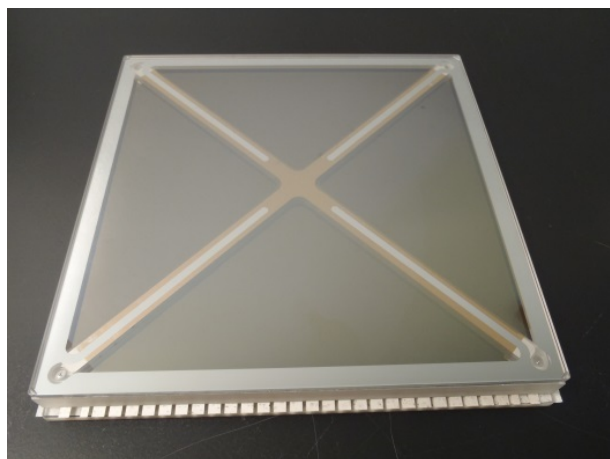


Fig. 11: 20 cm sealed tube “LAPPD” detector with a bialkali photocathode and 20 cm ALD borosilicate MCP pair (20 $\mu$ m Pores, 60:1 l/d, 13 $^\circ$  bias) with a strip-line anode.

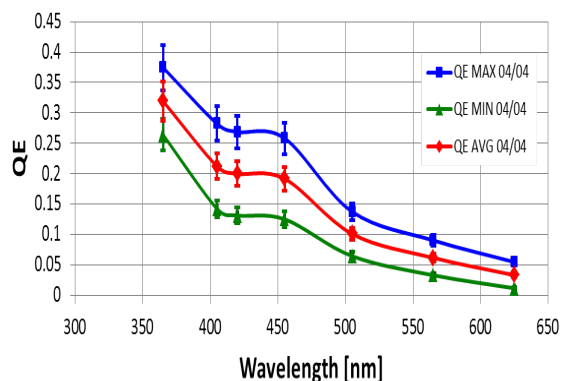


Fig. 12: Quantum efficiency of a 20 cm sealed tube bialkali photocathode ALD MCP detector (Fig. 11) at several positions on the face of the detector.

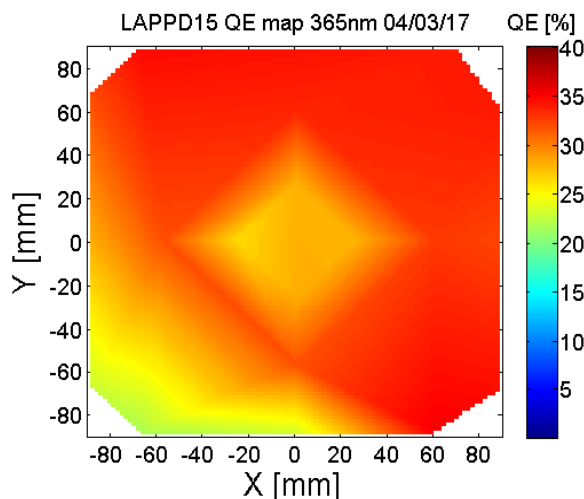


Fig. 13: 20 cm bialkali photocathode quantum efficiency uniformity as a function of position for 365 nm light.

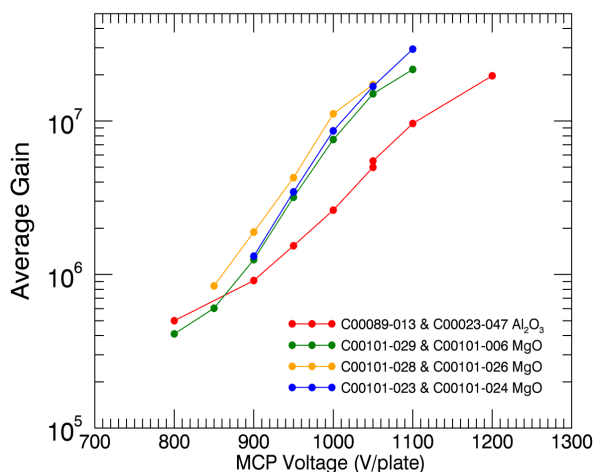


Fig. 14: Gain/voltage characteristic for pairs of 20 cm ALD MCPs with MgO or Al<sub>2</sub>O<sub>3</sub> secondary emissive layers.

The event timing resolution of these large devices has been previously assessed and for laser pulses of  $\sim 10$  e-, the timing jitter is a few hundred picoseconds (Fig. 15). More recent data [21] for completed sealed tubes shows a few hundred ps for single photoelectron events and  $<75$  ps for multiple photoelectron pulses. Adaptations of the LAPPD tube design can be envisaged. The strip anode has limited spatial resolution, but high timing resolution is appropriate for RICH applications. Other readouts (XS) could be employed with applications in astronomy and remote sensing.

### 3.2 Planacon Tubes with ALD Borosilicate Substrate Microchannel Plates

The Photonis Planacon [19] is a useful sealed detector format ( $\sim 50$  mm active area) to test basic functional parameters of new technologies. This includes photocathode, MCP and readout developments. One example is the variety of photocathodes and their optimizations are very dependent on the application. Traditionally the NUV-solar blind regime has been accommodated by CsTe or RbTe semitransparent photocathodes. Recently work with GaN [7], [18] has offered an alternative in both semitransparent and opaque configurations. We have recently begun to explore blue optimized bialkali photocathodes as another option. Initial two attempts (Fig. 16) have not achieved the 30% QE peak expectation for bialkalis, but the maintenance of high NUV QE and the steep response drop-off at 350 nm is a useful demonstration.

A Planacon with a 32 x 32 anode pad array, two 10  $\mu$ m pore ALD MCPs with 60:1 l/d and 8 $^\circ$  pore bias and a conventional bialkali cathode has been built (Fig. 17). The photocathode uniformity was good, and the initial quantum efficiency was close to the standard production expectations [22]. Over a 36 month period our measurements (Fig. 18) show no significant degradation of the photocathode. Further devices are planned with newer ALD MCP iterations, optimizations of the bialkali photocathode, a MgF<sub>2</sub> entrance window and inclusion of a XS anode. The materials used

to make the XS anodes for sealed tube applications are different than open face devices. In this case we employ ceramics for the substrates and insulating layers [23]. Our ceramic XS anode with 47mm field of view has previously achieved resolution of 20  $\mu\text{m}$  FWHM [23] with good image linearity and is a baseline for Planacon use.

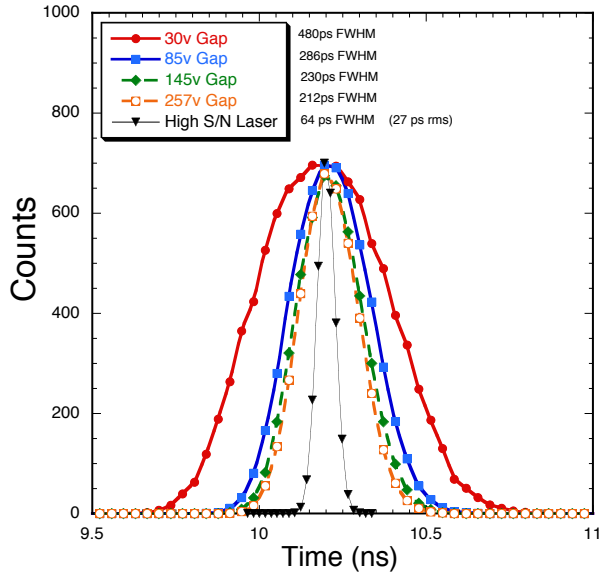


Fig. 15. Time stamp jitter distributions for detected laser pulses (80 ps laser @ 610 nm, 10 kHz), 20 cm detector with 20  $\mu\text{m}$  pore ALD MCP pair and bialkali cathode (gap ~1.5 mm). High S/N laser is ~150e<sup>-</sup>.

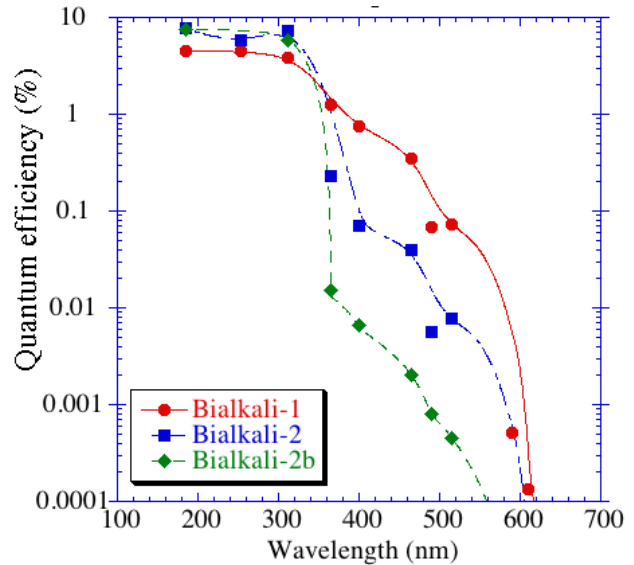


Fig. 16: Quantum efficiency for two preliminary tests of a UV optimized bialkali photocathode, deposited on an MgF<sub>2</sub> window as a semitransparent layer. Bialkali-2 was hot (>150°C) but 2b and 1 were at room temperature.

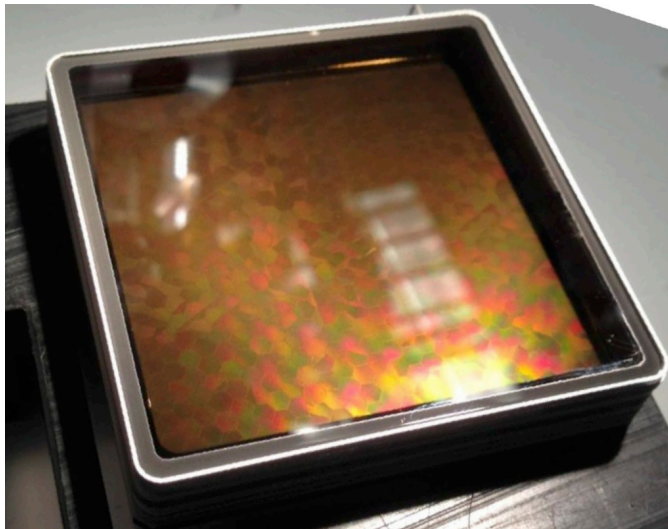


Fig. 17: Planacon 50 mm detector with a bialkali cathode and a pair of 53 mm, 10  $\mu\text{m}$  pore, 60:1 L/d, 8° bias ALD borosilicate substrate MCPs, 32 x 32 anode array.

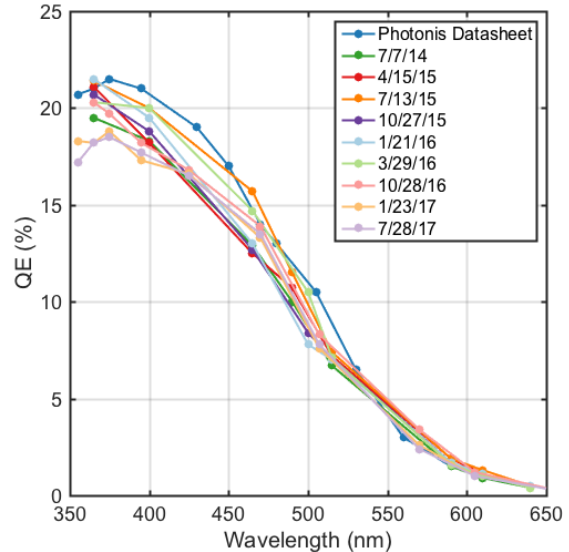


Fig. 18: Bialkali cathode quantum efficiency over 36 months for a Planacon with a pair of 53 mm, 10  $\mu\text{m}$  pore, 60:1 L/d, 8° bias ALD borosilicate substrate MCPs.

#### 4. ACKNOWLEDGEMENTS

We acknowledge the efforts of J. Hull, J. Tedesco, T. Curtis, N. Darling, Photonis – (France & USA), and Incom Inc. for their assistance. This work was supported by NASA grants NNG11AD54G & NNX14AD34G and DOE grant DE-SC0011262.

#### 5. REFERENCES

- [1] O. H. W. Siegmund, P. N. Jelinsky, S. R. Jelinsky, J. M. Stock, J. S. Hull, D. L. Doliber, J. Zaninovich, A. Tremsin, and K. E. Kromer, “High-resolution cross delay line detectors for the GALEX mission,” *Proc. SPIE*, vol. 3765, pp. 429–440, 1999.
- [2] J. Vallerga, J. Zaninovich, B. Welsh, O. H. W. Siegmund, J. McPhate, J. Hull, G. Gaines, and D. Buzasi,

- “The FUV detector for the cosmic origins spectrograph on the Hubble Space Telescope,” *Nucl. Instr. Meth. Phys. Res. A*, vol. 477, no. 1, pp. 551–555, 2002.
- [3] O. H. W. Siegmund, J. McPhate, A. Tremsin, J. Vallergera, B. Y. Welsh, and J. M. Wheatley, “High time resolution astronomical observations with the Berkeley Visible Image Tube,” *AIP Conf. Proc.*, vol. 984, pp. 103–114, 2008.
- [4] W. Priedhorsky and J. J. Bloch, “Optical detection of rapidly moving objects in space,” *Appl. Opt.*, vol. 44, no. 3, pp. 423–433, 2005.
- [5] O. H. W. Siegmund, J. Vallergera, P. Jelinsky, X. Michalet, and S. Weiss, “Cross delay line detectors for high time resolution astronomical polarimetry and biological fluorescence imaging,” *IEEE Nucl Sci Conf R*, vol. 1, pp. 448–452, 2005.
- [6] O. H. W. Siegmund, J. Vallergera, A. Tremsin, J. McPhate, and B. Welsh, “Optical Photon Counting Imaging Detectors with Nanosecond Time Resolution for Astronomy and Night Time Sensing,” *Proc AMOS*, 2011.
- [7] O. H. W. Siegmund, J. S. Hull, A. Tremsin, J. B. McPhate, and A. M. Dabiran, “Gallium nitride photocathodes for imaging photon counters,” *Proc. SPIE*, vol. 7732, pp. 77324T–77324T–9, Jul. 2010.
- [8] O. H. W. Siegmund, J. B. McPhate, S. R. Jelinsky, J. Vallergera, A. Tremsin, R. Hemphill, H. J. Frisch, R. G. Wagner, J. Elam, and A. Mane, “Large Area Microchannel Plate Imaging Event Counting Detectors with Sub-Nanosecond Timing,” *IEEE Trans. Nucl. Sci.*, vol. 60, no. 2, pp. 923–931, 2013.
- [9] C. Ertley, O. H. W. Siegmund, J. Schwarz, A. U. Mane, M. J. Minot, A. O’Mahony, C. A. Craven, and M. Popecki, “Characterization of borosilicate microchannel plates functionalized by atomic layer deposition,” *Proc. SPIE*, vol. 9601, pp. 96010S–96010S–10, 2015.
- [10] O. H. W. Siegmund, N. Richner, G. Gunjala, J. B. McPhate, A. Tremsin, H. J. Frisch, J. Elam, A. Mane, R. Wagner, C. A. Craven, and M. J. Minot, “Performance characteristics of atomic layer functionalized microchannel plates,” *Proc. SPIE*, vol. 8859, p. 88590Y, 2013.
- [11] O. H. W. Siegmund, C. Ertley, C. A. Craven, J. Vallergera, M. Popecki, A. O’Mahony, and M. J. Minot, “High Speed Large Format Photon Counting Microchannel Plate Imaging Sensors,” *Proc AMOS*, vol. 1, p. 94, 2015.
- [12] J. Vallergera, J. McPhate, A. Tremsin, O. H. W. Siegmund, R. Raffanti, H. Cumming, A. Seljak, V. Virta, and G. Varner, “Development of a flight qualified 100 x 100 mm MCP UV detector using advanced cross strip anodes and associated ASIC electronics,” *Proc. SPIE*, vol. 9905, pp. 99053F–99053F–12, 2016.
- [13] J. Vallergera, R. Raffanti, M. Cooney, H. Cumming, G. Varner, and A. Seljak, “Cross strip anode readouts for large format, photon counting microchannel plate detectors: developing flight qualified prototypes of the detector and electronics,” *Proc SPIE*, vol. 9144, p. 91443J, 2014.
- [14] O. H. W. Siegmund, J. McPhate, H. Frisch, J. Elam, A. Mane, R. Wagner, and G. Varner, “Large Area Flat Panel Imaging Detectors for Astronomy and Night Time Sensing,” *Proc. AMOS*, 2013.
- [15] O. H. W. Siegmund, J. McPhate, T. Curtis, S. Jelinsky, J. Vallergera, J. Hull, and J. Tedesco, “Ultraviolet imaging detectors for the GOLD mission,” *Proc. SPIE*, vol. 9905, pp. 99050D–99050D–10, 2016.
- [16] O. H. W. Siegmund, C. Ertley, J. Vallergera, E. Schindhelm, A. Harwit, B. Fleming, K. France, J. Green, S. R. McCandliss, and W. M. Harris, “Microchannel Plate Detector Technology Potential for LUVVOIR,” *Proc. SPIE*. In Press.
- [17] C. Ertley, O. H. W. Siegmund, A. Tremsin, J. Hull, A. O’Mahony, M. Minot, and C. Craven, “Microchannel Plate Imaging Detectors for High Dynamic Range Applications,” *IEEE Trans. Nucl. Sci.*, vol. PP, no. 99, pp. 1–1, 2017.
- [18] A. Tremsin, J. S. Hull, O. H. W. Siegmund, J. B. McPhate, J. Vallergera, A. M. Dabiran, A. Mane, and J. Elam, “Opaque gallium nitride photocathodes in UV imaging detectors with microchannel plates,” *Proc. SPIE*, vol. 8859, p. 88590X, 2013.
- [19] Photonis, “PLANACON™ Photodetector,” <https://www.photonis.com/en/product/planacon%E2%84%A2-photodetector>. Jul. 2015.
- [20] O. H. W. Siegmund, C. D. Ertley, S. R. Jelinsky, J. B. McPhate, J. Tedesco, M. J. Minot, A. O’Mahony, and C. A. Craven, “Very large area 20cm x 20cm flat panel phototubes using ALD microchannel plates,” *Proc. IEEE NSS*, 2015, pp. 1–7.
- [21] B. W. Adams, A. Elagin, H. J. Frisch, R. Obaid, E. Oberla, A. Vostrikov, R. G. Wagner, J. Wang, and M. Wetstein, “Timing characteristics of Large Area Picosecond Photodetectors,” *Nucl. Instr. Meth. Phys. Res. A*, vol. 795, pp. 1–11, Sep. 2015.
- [22] O. H. W. Siegmund, C. Ertley, and J. Vallergera, “High Time Resolution Photon Counting 3D Imaging Sensors,” *Proc. AMOS*, p. 5, 2016.
- [23] O. H. W. Siegmund, A. Tremsin, and J. Vallergera, “Development of cross strip MCP detectors for UV and optical instruments,” *Proc. SPIE*, vol. 7435, pp. 74350L–74350L–10, 2009.